

# Molecular Communications Loss Budget for tsRNA Detection in the Brain

Aiman Khalil, *Student Member, IEEE*, Kurt J. A. Pumares, *Student Member, IEEE*, Anne Skogberg, Pasi Kallio, Deirdre Kilbane, *Member, IEEE*, and Daniel P. Martins, *Member, IEEE*

**Abstract**—Molecular communication (MC) is an emerging framework enabling communication among biological cells and bio-nanomachines at nano and micro scales through biochemical molecules. Recent studies have identified exosomal transfer RNA-derived small RNAs (tsRNAs) as potential biomarkers for epilepsy. Consequently, researchers are exploring innovative methods to predict epileptic seizures through tsRNA measurements, using implantable micro/nanoscale biosensors. This paper presents a propagation model for biomarkers in a heterogeneous fluidic environment, composed of the brain extracellular space (ECS), a polyethersulfone (PES) hollow fiber tube, and a hydrogel (e.g. collagen) containing bioengineered sensing cells for biomarker detection. Our proposed model aims to support the design of biosensing devices for epileptic seizure prediction by characterizing the propagation of biomarkers released from neuronal cells in the brain ECS to the implant. We analyse the communication performance of the proposed system by evaluating propagation loss under varying conditions—brain ECS tortuosity, fiber membrane thickness, permeability, and bioengineered sensing cell density. Furthermore, we develop an MC link budget to assess communication between exosomal tsRNA biomarkers and bioengineered sensing cells, based on received biomarkers. We observed an approximate 8-fold loss in received signal strength, highlighting the impact of MC communication media physicochemical characteristics for accurately designing devices to predict epileptic seizures.

**Index Terms**—heterogenous channel, loss budget, epilepsy biomarker, bioengineered implants, neuronal communications, neuroengineering

## I. INTRODUCTION

**E**PILEPSY is a chronic neurological disorder that affects more than 50 million people worldwide [1, 2]. This disorder is characterized by recurring seizures resulting from abnormal and synchronous firing of neurons within the brain, which can severely affect people’s lives [3]. During the onset of an epileptic seizure, various biomarkers are released from brain cells, such as miRNAs and IL-1 $\beta$  [4]. From those, transfer RNAs (tRNA) fragments (tsRNA), have emerged as a novel

type of biomarker associated with epilepsy [5]. They have also been identified in exosomes [6] released from neurons and other cell types such as human glioma stem cells [7, 8]. Exosomal tsRNAs are released during epilepsy as part of the neuronal stress response, often triggered by hypoxia, oxidative damage, or other adverse conditions. This stress leads to the cleavage of tRNAs into smaller fragments, mediated primarily by ribonucleases such as angiogenin and Dicer [6, 9]. Once released into the extracellular environment, these tsRNA fragments can contribute to the general pathophysiology of epilepsy. Specifically, researchers have observed elevated tsRNA levels in individuals with epilepsy compared to healthy controls, suggesting their potential as diagnostic and prognostic biomarkers [5]. Hence, micro and nanoscale biosensors are targeting these biomarkers as early indicators of the occurrence of epileptic seizures.

Recent advancements in material engineering and nanotechnology have facilitated the development of micro/nanoscale implantable biosensors. These sensors are capable of detecting biomarkers associated with neurological diseases, such as  $\alpha$ -synuclein for Parkinson’s disease and tsRNA biomarkers for epilepsy [10, 11]. Despite that, the complex brain microenvironment during pathological and physiological processes still poses a challenge for the design of implantable biosensors. These challenges include requirements for molecular selectivity, sensitivity, and biocompatibility, all of which can significantly impact the effectiveness of implantable biosensors. To further advance this field (including the early prediction of diseases, such as epilepsy), novel and innovative solutions are fundamental to overcome such challenges. This includes optimizing both the physical and logical design of bioengineered implants. For instance, incorporating biological materials into implant designs can enhance biocompatibility. Additionally, integrating biomolecule detection capabilities—such as graphene-based sensors to detect neurotransmitters like dopamine can be crucial for diagnosis and monitoring neurological disorders, such as Parkinson’s disease [12, 13]. Furthermore, when these novel implants are capable of detecting disease related biomarkers, they can be applied to predict chronic illnesses [12]. Therefore, the further understanding on the bioavailability of these biomarkers and how they are transported within biological spaces (e.g., human body) is essential for the development of effective implantable biosensors. In this paper, we utilise a MC system to investigate the transport of exosomal tsRNA from neuron cells towards an implantable biosensor. Molecular communication (MC) is an interdisciplinary communication paradigm that investigates the exchange of molecules among micro/nanoscale entities (either natural or artificial) [14]. We applied this framework to characterize the molecular propagation through heterogeneous media and the effects on the bioavailability of exosomal tsRNA inside of

A. Khalil, and K. J. A. Pumares are with the Walton Institute for Information and Communication Systems Science, South East Technological University, Waterford, X91 P20H, Ireland. Corresponding author (A. Khalil): aiman.khalil@waltoninstitute.ie

Deirdre Kilbane is with the FutureNeuro SFI Research Centre, Walton Institute for Information and Communication Systems Science, South East Technological University, Waterford, X91 P20H, Ireland.

A. Skogberg and P. Kallio are with the BioMediTech Institute and Faculty of Medicine and Health Technology, Tampere University, Korkeakoulunkatu 3, 33720 Tampere, Finland.

D. P. Martins is with the School of Computer Science and Electronic Engineering, University of Essex, Wivenhoe, CO4 3SQ Colchester, United Kingdom.

This research was funded by the EU under grant No. 964712 (EU-H2020-FETOpen PRIME A Personalised Living Cell Synthetic Computing Circuit for Sensing and Treating Neurodegenerative Disorders) and has emanated from research supported in part by a research grant from Science Foundation Ireland (SFI) under Grant Number 21/RC/10294\_P2 and co-funded under the European Regional Development Fund and by FutureNeuro industry partners.

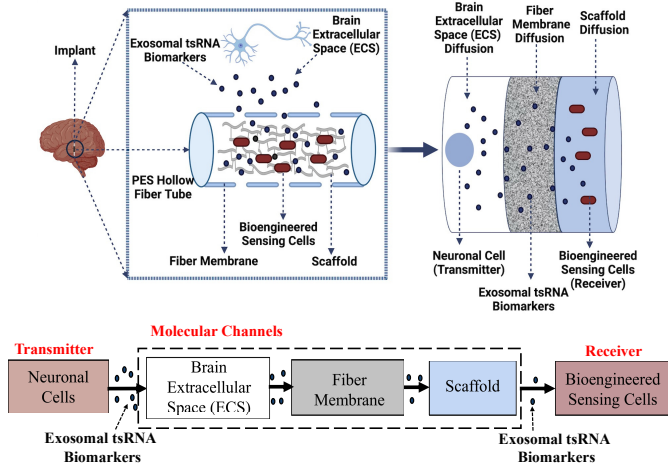


Fig. 1: Schematic illustration of MC between cells in a heterogeneous fluidic environment.

the implantable biosensor. In this study, the heterogeneous communication channels are composed of three fluids used for the transport of exosomal tsRNA, while the implantable biosensor is composed of bioengineered sensing cells encapsulated inside the PES hollow fiber tube. The primary challenges associated with the efficacy of an implantable biosensor in the brain is the complexity of the biological environment where it sits and its physicochemical properties, which can impact molecule propagation and consequently reduce the bioavailability of exosomal tsRNA at the bioengineered sensing cells. Therefore, this paper aims to provide a further understanding on the molecular channel properties affecting the exosomal tsRNA propagation towards the implantable biosensor, and provide a simple method to assess the molecular concentration losses that can reduce the sensing performance of the system. By investigating the interplay between epileptic biomarkers diffusion and device characteristics, our model may offer valuable insights into optimizing biosensor design and improving the accuracy and reliability of micro/nanoscale epileptic seizures prediction systems.

Previous research in similar topics (i.e., molecular propagation in the brain) have been conducted using MC channels. However, many of them simplify the molecular channel as a single uniform channel characterized by a constant diffusion coefficient [15–17]. In other studies [18, 19], the multi-layer molecular medium has been investigated primarily to determine the average effective diffusion coefficient. These studies substituted the individual layers’ diffusion coefficients with the calculated average, which is then incorporated into expression for molecular concentration of a single-layer medium. In addition to their simplified approach, these models lack accuracy in representing real multi-layer biological environments, especially under transient conditions. To address the limitation of the approach, a recent modeling approach was presented in [20], where a composite diffusive molecular channel was developed with distinct diffusion properties. While in that work the authors have considered the physicochemical properties of individual channels to some extent to evaluate their system performance, we introduce a novel application involving the diffusion of epileptic biomarkers towards bioengineered cells for epileptic seizures

prediction, which has not been explored in prior literature. We also introduce a concept of heterogeneous molecular channel which comprises of three channels including brain ECS, fiber membrane (referred to as the membrane in subsequent sections) and scaffold (hydrogel) as shown in Fig. 1. Additionally, we delve deeper into the impact of these physicochemical properties on propagation loss, thereby impacting the sensitivity of epileptic seizures prediction, offering a more comprehensive understanding of their effects on communication performance compared to existing studies. Furthermore, we propose a link budget equation to assess the performance of our MC system, in terms of biomarkers received by the bioengineered sensing cells. Our main contributions to this research work are as follows:

- **Modeling and characterizing epileptic biomarker propagation as a MC system:** The tsRNA propagation in a heterogeneous media is represented using MC concepts, and a propagation loss metric is utilised to assess the performance of the proposed system.
- **Analyse the impact of physicochemical characteristics on tsRNA bioavailability:** We analyse the impact of various physicochemical properties of brain ECS and the implantable biosensor to observe their influence on the exosomal tsRNA bioavailability reduction, which induces losses to the proposed MC system. Our numerical analysis is based on the data collected from an experimental setup we have devised.
- **Development of MC Link Budget:** We propose a link budget equation to evaluate the communication performance of the system, in terms of received exosomal tsRNA concentration by the implantable biosensor. This budget provides insights into optimizing the design of bioengineered devices to ensure efficient propagation and bioavailability of epileptic biomarker signals.

The rest of the paper is organized as follows. In Section II, we detail the MC model and implantable biosensor physical design. We describe the heterogeneous media in Section III, the link budget formulation in Section IV-D. Our results are presented in Section IV and our conclusions in Section V.

## II. SYSTEM MODEL

The proposed system model composed of three biological fluidic propagation regions namely, Brain ECS, Membrane and the Scaffold region utilising target molecules (i.e. exosomal tsRNA biomarkers) as illustrated in Fig. 1. Each region, depicted in Fig. 1 is connected through MC links based on free diffusion. In the proposed model, the whole process starts with the release and propagation of exosomal tsRNA biomarkers from the neuronal cells, under epileptic seizures, through the fluidic environment to the bioengineered sensing cells. These bioengineered sensing cells are encapsulated inside the hollow fiber tube and entrapped in the scaffold region to detect the incoming molecules from the brain ECS. Both regions (brain ECS and scaffold) communicate with each other through a porous membrane wall. This membrane wall is built with an organic compound (e.g. PES) that allows the molecules to flow from the brain ECS to the scaffold region. In this paper, we consider that the interface between different regions is permeable, allowing molecules to pass through without undergoing any physical or chemical reactions [21]. Also, we assume that scaffold boundary is impermeable to the cells and the cells are firmly adhered to the scaffold.

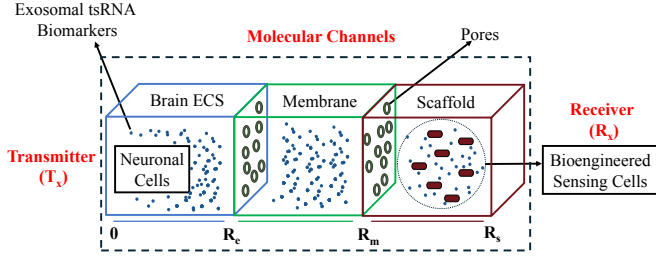


Fig. 2: Molecular Communication (MC) propagation model for biological heterogeneous fluidic environment.

From the perspective of MC as depicted in Fig. 2, we define the neuronal cells as the point-source MC transmitter ( $T_x$ ) positioned at the point  $r = r_0$  in the Brain ECS, which emits the exosomal tsRNA biomarkers ( $Q$ ) (i.e., the molecular signal) instantaneously at the time  $t = 0$  s. The MC channel through which this signal propagates is a heterogeneous fluidic medium composed of three different regions: brain ECS, the membrane of a PES hollow fiber tube, and the scaffold (hydrogel) containing the bioengineered sensing cells (i.e., the molecular receiver -  $R_x$  responsible for the detection of the incoming exosomal tsRNAs biomarkers). Each of these regions have well-defined physicochemical properties that directly affect the propagation of the molecular signal, which follows a Brownian motion (a comprehensive overview for each region is provided in Section III).

The hollow fiber tube is made of PES, which is known to provide tissue biocompatibility, cytocompatibility, and permeability for the influx and efflux of biomolecules (see Fig. 3). The tube selected for the wet lab experiments has a  $300 \mu\text{m}$  inner diameter and a  $470 \mu\text{m}$  outer diameter resulting in a wall thickness of  $85 \mu\text{m}$  with a pore size of  $200 \text{ nm}$ . Using a  $31\text{G}$  syringe needle, the tube is filled with a suspension containing bioengineered sensing receiver cells and  $1.5 \text{ mg/mL}$  Collagen Type I hydrogel. The ends of the tube are closed using heat-sealing, where a sharp heated tip (approximately  $200^\circ\text{C}$ ) is used to simultaneously cut and seal the tube. The PES tubes are placed between a polydimethylsiloxane sheet (PDMS) and a polyvinylidene fluoride (PVDF) sheet during heat-sealing. The PDMS sheet is soft to keep the tube in place whereas the PVDF sheet protects the tube from a direct contact of the heated tip.

### III. HETEROGENEOUS MC CHANNELS

Epileptic biomarkers (i.e., exosomal tsRNAs) released from the neuronal cells travel through a complex biological environment including brain ECS, the membrane and scaffold of the hollow fiber tube to reach the targeted bioengineered sensing cells. Here we defined each one of these diffusion media as a MC channel, and this propagation process is influenced by the various physicochemical characteristics of the heterogeneous MC channels. For instance, the molecular diffusion through the brain ECS is affected by the tortuosity and volume fraction, which represents the percentage of the total brain tissue volume that is accessible to the exosomal tsRNAs. The hindrance to the molecular propagation leads to an effective diffusion coefficient, which is lower than the free diffusion coefficient ( $D$ ) for the

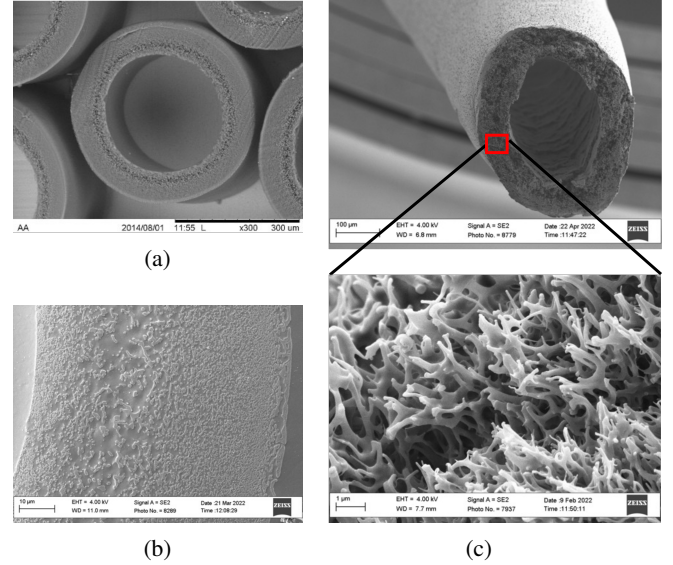


Fig. 3: (a) Cross-section of hollow fiber tubes. (b) Cross-section from a hollow fiber membrane wall. (c) Expanded view of the hollow fiber wall.

exosomal tsRNA biomarkers. In the context of neurobiology, the tortuosity is calculated as [22],

$$\lambda = \sqrt{\frac{D}{D^*}}, \quad (1)$$

where  $D^*$  represents the effective diffusivity of exosomes within the extracellular matrix of the brain. The tortuosity of this matrix remains relatively consistent, typically  $\lambda \approx 1.6$  [22, 23].

When the exosomal tsRNAs enter the membrane of the hollow fiber tube from the brain ECS, their movement is influenced by the morphological structure of the membrane such as thickness, permeability and diffusion coefficient [24, 25]. The entry of biomarkers primarily occurs through the side walls of the hollow fiber tube, reflecting our experimental setup, where the ends of the tube are sealed, restricting molecular entry from those areas. Additionally, interactions between biomarkers and the porous network of the membrane, including factors like void spaces (porosity) and the tortuous path length (tortuosity), significantly impact this molecular transport. Finally, to continue their movement to the targeted site, the exosomal tsRNAs must escape through the pores in the hollow fiber tube membrane into the cell culture medium compartment (i.e., scaffold), where the bioengineered sensing cells are located near the inner membrane wall. The bioavailability of exosomal tsRNAs in the scaffold region is influenced by factors such as the diffusion coefficient in the hydrogel-medium suspension (e.g., collagen), bioengineered cell density and the rate at which they are taken up by the bioengineered sensing cells (i.e., the uptake rate). Consequently, these factors collectively dictate the complex dynamics of exosomal tsRNA transport through the heterogeneous MC channel, highlighting the interplay between structural elements and their effects on the MC link.

The following sections detail our proposed mathematical model for the overall exosomal tsRNA transport through the heterogeneous MC channels, where we consider their various physicochemical features and their effects on the bioavailability of exosomal tsRNA. Therefore, we consider that each region of

the MC channel is finite with a defined length: ECS starts at the point zero and finishes at length  $R_e$ , from  $R_e$  to  $R_m$  for the membrane and from  $R_m$  to  $R_s$  for the scaffold. Additionally, we adopt a cylindrical coordinate system to derive a mathematical solution for the hollow fiber tube, while employing a spherically symmetric coordinate system for the brain ECS that depends only on the radial distance. Table I summarizes the notation used in the subsequent subsections.

### A. Transport Across the Brain ECS Region

For the exosomal tsRNA transport through the brain ECS, we consider the modified version of Fick's second law of diffusion as demonstrated by [22], which is represented as follows,

$$\frac{\partial C_e}{\partial t} = \frac{D_e}{\lambda_e^2} \nabla^2 C_e - v_e \cdot \nabla C_e + \frac{S}{\alpha} - \frac{f(C_e)}{\alpha}, \quad (2)$$

where  $C_e$  represents the concentration of exosomal tRNAs in the brain ECS,  $S$  is the source term,  $f(C_e)$  represents the uptake by other cells or loss of exosomal tsRNAs through degradation or enzymatic processes,  $\alpha$  denotes the proportion of the brain ECS volume, while  $\lambda_e$  describes how tortuous or convoluted the brain ECS pathways are within the brain, and finally  $v_e$  represents the velocity of the fluid flow in the system. In our case, the brain ECS is a diffusion-only channel we ignored the advection term  $v_e \cdot \nabla C_e$ . Also, we omit the uptake function from the equation, assuming that the neuronal cells act as a point-source for releasing exosomal tRNAs and do not participate in their uptake and degradation. Our aim is to quantify the exosomal tsRNA concentration in the brain ECS without considering any uptake processes. Furthermore, we consider that the molecular diffusion occurs in a spherical symmetric bounded environment, and the bioavailability of exosomal tsRNAs,  $C_e(r, t)$  in the brain ECS is subjected to the influence of tortuosity and exosome diffusion coefficient in this medium  $D_e$ . By considering the biomarkers emission rate as an impulsive point-source  $S(r, t)$ , we transform (2) as follows,

$$\frac{\partial C_e(r, t)}{\partial t} = \frac{D_e}{\lambda_e^2} \frac{\partial^2 C_e(r, t)}{\partial r^2} + S(r, t), \quad (3)$$

where,

$$S(r, t) = Q \cdot \delta(r - r_0) \cdot \delta(t - t_0), \quad (4)$$

$\delta(\cdot)$  is the Dirac delta function,  $t$  stands for time,  $r$  is the length of the MC channel. In our model, the number of exosomes released into brain ECS for propagation at time  $t_0$  and location  $r_0$  follows a Poisson distribution with a mean  $Q$ . The parameter, such as the number of released molecules in Table I, is chosen to observe significant variations in the received exosomal tsRNA concentration. The thickness of the brain ECS (i.e., the propagation distance from the neuronal cell to the device) is estimated based on literature indicating that it falls within a range where significant cellular interactions have been observed around implants [26]. The following initial and boundary conditions are considered,

$$\begin{cases} C_e(r_0, t \rightarrow t_0) = Q\delta(r - r_0), \\ D_e \frac{\partial C_e(r, t)}{\partial r} = D_m \frac{\partial C_m(r, t)}{\partial r} \quad \text{at } r = R_e, \end{cases} \quad (5)$$

where ( $r = R_e$ ) is the interface between the brain ECS and the membrane region, considering that the bioavailability of exosomal tsRNA remains continuous at the interface.

### B. Transport Across the Membrane Region

In this section, we describe the modeling of the exosomal tsRNA transport through the hollow fiber tube's membrane. This structure is a PES hollow fiber tube built to be biocompatible with the brain environment and to contain the bioengineered sensing cells. The transport of biomarkers through this membrane is influenced by its morphological features, including geometry, porosity, tortuosity, and permeability. In the membrane region, we assume that no chemical reaction occur [21], and the exosomal tsRNAs permeates through the membrane by diffusion process [24] with a diffusion coefficient  $D_m$ . The hollow fiber tube is cylindrical in shape, as shown in Fig. 3b, we considered the molecular diffusion only depends on the radial distance and not on the azimuthal angle and axial position, i.e.,  $\frac{\partial C_m(r, \varphi, z, t)}{\partial \varphi} = 0$  and  $\frac{\partial C_m(r, \varphi, z, t)}{\partial z} = 0$ , respectively. In this context, the majority of molecules are primarily sourced from the direction of the point-source in the brain ECS. In our wet-lab experimental setup, bioengineered sensing cells are positioned near the inner membrane layer of the hollow fiber tube and the ends of tube are closed, making radial transport the primary mechanism for delivering biomarkers to these bioengineered sensing cells. This positioning facilitates effective interactions with the bioengineered sensing cells, essential for effective detection and response. This approach aligns with similar modeling approaches in the literature that use radial flow models [27–30]. In this case, the transport behaviour in the membrane region is governed by the following equation,

$$\frac{\partial C_m(r, t)}{\partial t} = D_m \left[ \frac{\partial^2 C_m(r, t)}{\partial r^2} + \frac{1}{r} \frac{\partial C_m(r, t)}{\partial r} \right], \quad (6)$$

where  $C_m(r, t)$  is the exosomal tsRNAs concentration in the membrane region.

By using the principles of transport within porous materials [24, 31], we can derive an expression for  $D_m$  based on membrane characteristics [24, 32] as,

$$D_m = \frac{\phi}{\lambda_m} \cdot D_s, \quad (7)$$

where,  $\phi$  is the PES porosity,  $\lambda_m$  is the membrane tortuosity and  $D_s$  is the diffusion coefficient in scaffold region. The PES porosity is a measure of the material's ability to allow molecules to pass through it. This structural feature is mathematically modeled by the ratio of volume of voids and the total volume of the material [14, 24]. Here, we calculate the volume of voids based on the mean pore size  $r_p = \frac{d_p}{2}$ , the number of surface pores  $n_p$  and the height  $h$ , of the hollow fiber tube as  $V_p = n_p \times \pi \times (r_p)^2 \times h$ . The solid volume of hollow fiber tube is calculated as  $V_m = \pi ((r_{out}^m)^2 - (r_{in}^m)^2) h$ , where  $r_{in}^m$  and  $r_{out}^m$  are the inner and outer radii of the hollow fiber tube (i.e. device), respectively. Therefore, we model the total porous membrane volume based on [33][34] as  $V_t = V_m + V_p$  and define the PES porosity as,

$$\phi = 1 - \frac{V_p}{V_t}. \quad (8)$$

The membrane tortuosity ( $\lambda_m$ ) is a measure of the geometric complexity of a porous medium. Here we assume  $\lambda_m = 2$  considering  $d_p = 200$  nm and  $n_p = 400$ , which are the same values found in [35, 36].

The interface between two diffusive environments with different diffusion coefficients requires a flow continuity condition.

Therefore, we define the following boundary conditions for the interface between the brain ECS and the membrane regions ( $r = R_e$ ) based on [20, 24, 37] as,

$$\begin{cases} D_m \frac{\partial C_m(r, t)}{\partial r} = D_e \frac{\partial C_e(r, t)}{\partial r}, \\ C_m(r, t) = P_m C_e(r, t), \end{cases} \quad (9)$$

where  $P_m = D_m/R_m$  is the PES membrane effective permeability (given in  $\mu\text{m/s}$ ),  $R_m$  and  $D_m$  refers to thickness and effective diffusivity of the membrane, respectively.

### C. Transport Across the Scaffold Region

The scaffold region is the medium inside of the hollow fiber tube ( $R_m < r < R_s$ ). It is composed of a hydrogel and it houses the bioengineered sensing cells. In this region, the propagation of exosomal tsRNA biomarkers is characterised by the diffusion coefficient and consumption by the bioengineered sensing cells, which is modelled via diffusion-reaction equation [38] as follows,

$$\frac{\partial C_s(r, t)}{\partial t} = D_s \left[ \frac{\partial^2 C_s(r, t)}{\partial r^2} + \frac{1}{r} \frac{\partial C_s(r, t)}{\partial r} \right] - R^{\text{cell}}, \quad (10)$$

where,  $C_s(r, t)$  is the molecular concentration of exosomal tsRNAs in scaffold region,  $D_s$  is the diffusion coefficient in the scaffold region, and is given by the Stokes-Einstein equation [20] as,

$$D_s = \frac{k_B T}{6\pi\eta a}. \quad (11)$$

Here,  $k_B = 1.38 \times 10^{-23}$  J/K represents the Boltzmann constant,  $T = 310.15$  denotes the absolute temperature of the medium in Kelvin [39], and  $\eta = 0.01$  is the hydrogel (i.e., collagen) viscosity constant measured in  $\text{Pa} \cdot \text{s}$  [40], and  $a$  is the radius of the diffusing exosome. Furthermore,  $R^{\text{cell}}$  is the rate of exosomal tsRNAs consumption by the bioengineered sensing cells. This rate follows Michaelis-Menten kinetics, and it is a function of the maximum uptake rate ( $V_{\text{max}}$ ), the half saturation concentration ( $k_H$ ), and the cell seeding density ( $N_0$ ). Therefore,  $R^{\text{cell}}$  can be expressed as,

$$R^{\text{cell}} = V_{\text{max}} \cdot \frac{N_0 C_s(r, t)}{k_H + C_s(r, t)}. \quad (12)$$

Here,  $V_{\text{max}}$  (mol./cell·s) is calculated based on [41] as  $V_{\text{max}} = Q/N_0 \cdot t \cdot \mu\text{L}$ , where  $Q$  is the number of molecules,  $t$  is time in seconds,  $N_0$  (cells/ $\mu\text{L}$ ) is the number of biosensing cells in the medium volume ( $\mu\text{L}$ ).

We assume that the exosomal tsRNA bioavailability remains continuous at the interface between the inner radius of the membrane and the scaffold region ( $r = R_m$ ). Therefore,

$$\begin{cases} D_s \frac{\partial C_s(r, t)}{\partial r} = D_m \frac{\partial C_m(r, t)}{\partial r}, \\ C_s(r, t) = P_m C_m(r, t). \end{cases} \quad (13)$$

## IV. NUMERICAL RESULTS AND DISCUSSION

We evaluated the performance of the MC system through a comprehensive analysis of the parameters affecting the propagation loss and the MC link budget including: tortuosity, thickness, porosity, permeability, uptake rate and the bioengineered sensing cell densities. To ensure clarity in interpretation, targeted parameter simulations were conducted with other factors held

TABLE I: Values, definitions and sources for the parameters used to compute (1)-(18). Please note that the notation ‘‘mol.’’ is used as a shorthand for ‘‘molecules’’.

Parameter	Value	Description	Source
$Q$	700 mol.	# of released tsRNA	See section III-A
$R_e$	95 $\mu\text{m}$	Thickness of brain ECS	See section III-A
$R_m$	85 $\mu\text{m}$	Thickness of PES membrane	Experimental data
$R_s$	150 $\mu\text{m}$	Thickness of Scaffold (Hydrogel)	Experimental data
$D_e$	15 $\mu\text{m}^2/\text{s}$	Brain ECS diffusion coefficient	[23]
$\lambda_e$	1.67	Tortuosity of Brain ECS	[23]
$\lambda_m$	2	PES membrane tortuosity	[24]
$r_{\text{out}}$	235 $\mu\text{m}$	PES membrane outer radius	Experimental data
$r_{\text{in}}$	150 $\mu\text{m}$	PES membrane inner radius	Experimental data
$h$	7 mm	Height of device (Hollow fiber tube)	Experimental data
$N_0$	3000 cells/0.7 $\mu\text{L}$	Bioengineered sensing cells seeding density	Experimental data
$k_H$	$3.8 \times 10^{14}$ mol./ $\mu\text{L}$	Half-saturation constant	[42]

constant, as detailed in Table I. The simulations in this study were implemented using MATLAB<sup>®</sup> and Python. We used MATLAB<sup>®</sup> to run a finite difference method (FDM) algorithm to solve the partial differential equations (PDEs) governing molecular diffusion across the channel, while Python was used for calculating confidence intervals for the exosomal tsRNA concentration obtained in our analysis. We simulated 10 runs for each scenario to capture the variability in the release of exosomal tsRNA and obtain a robust estimation of its concentration profiles. Each one of them run for  $T = 500$  s with a time step of 0.01 s (these values were chosen to ensure a significant observation period and impactful variation on the exosomal tsRNA concentration).

### A. Impact of Physicochemical Factors on Molecular Propagation

As detailed in Section III, the exosomal tsRNA concentration is affected by the physicochemical properties of the different MC channels. Therefore, we first assess the temporal dynamics of the exosomal tsRNA propagation through the three regions (brain ECS, membrane and scaffold). Separate y-axes are used for each region to represent the varying concentration profiles, as shown in Fig. 4. Here, we considered the propagation distances and the physicochemical factors as presented in Table I (please note that the propagation distance are denoted as brain ECS, membrane and scaffold thickness). Exosomal tsRNA are initially released into the brain ECS at time  $t = 0$  s, and propagation is governed by continuity flux boundary conditions at the interfaces between the brain ECS, membrane and scaffold. Please note that the results shown in Fig. 4 is a superposition, in a single graph, of the temporal dynamics of exosomal tsRNA propagating through each communication channel. Each region has a distinct y-axis scale to reflect its specific peak concentration values. The differences in peak concentrations observed across regions are due to variations in propagation distances and diffusion coefficients. Specifically,

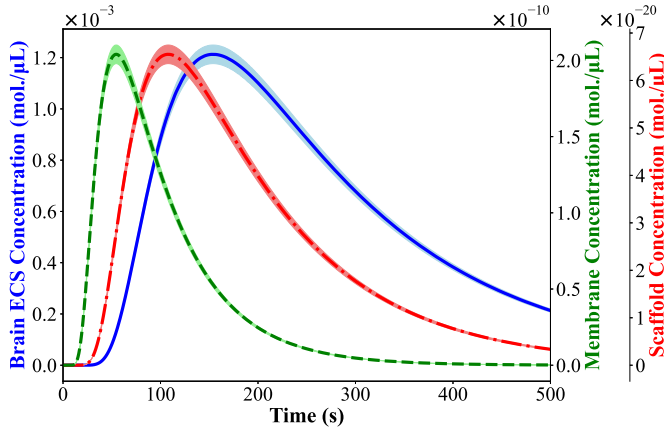


Fig. 4: Temporal evaluation of exosomal tsRNA propagation through the brain ECS, membrane, and scaffold. The graph shows a superposition of tsRNA propagation dynamics, highlighting variations in concentration profiles due to different propagation distances and diffusion coefficients. The plot illustrates the mean concentration profile along with a 95% confidence interval.

the brain ECS, with a propagation distance of  $95 \mu\text{m}$  and a relatively high diffusion coefficient, reaches its peak concentration at  $t = 180 \text{ s}$ , as shown on a y-axis scale of  $10^{-3} \text{ mol./}\mu\text{L}$ . Although the high diffusion coefficient facilitates rapid spreading of exosomal tsRNA, the longer distance results in a delayed peak. The membrane, with a shorter propagation distance of  $85 \mu\text{m}$  and slightly lower diffusion coefficient, reaches its peak at around  $t = 80 \text{ s}$ , due to the reduced distance allowing faster propagation. This results in a peak concentration measured on a y-axis scale of  $10^{-10} \text{ mol./}\mu\text{L}$ , which is lower than the peak concentration observed in the brain ECS. The scaffold, with a propagation distance of  $150 \mu\text{m}$  and a higher diffusion coefficient than the membrane, achieves its peak at  $t = 120 \text{ s}$  reflecting the faster propagation from the membrane but also accounts for the longer distance required for the molecules to traverse. The resulting peak concentration is measured on a y-axis scale of  $10^{-20} \text{ mol./}\mu\text{L}$ , which is lower than the peak concentration observed in the brain ECS and the membrane. Moreover, we can observe that for the first few seconds (between  $\approx 20 - 40 \text{ s}$ ), the concentration of exosomal tsRNA remain zero across all regions, representing the delay required by molecules to start to accumulate at the end of each region due to the molecule diffusion dynamics. Next, we varied the physicochemical factors of each MC channel and observed their impact on the exosomal tsRNA concentration in respect of time. The results obtained from this analysis are illustrated in Fig. 5, where exosomal tsRNA are released from a point-source in brain ECS and diffuses across each region toward their respective endpoints (i.e., the boundary or the beginning of another region). We have chosen these endpoints as observation locations for measuring exosomal tsRNA concentrations to understand the overall diffusion dynamics, which may, in turn, affect the detection capabilities and response of the bioengineered sensing cells. Note that the plots show a mean concentration profile with a 95% confidence interval (calculated using the method outlined in [43]) to represent the variance associated with our simulation.

For the brain ECS, we analysed the impact of tortuosity ( $\lambda_e$ ) and this medium thickness on the exosomal tsRNA propagation.

From equation (1), we observed an inversely proportional relationship between the effective diffusion coefficient and the brain ECS tortuosity, which also result in a delay in the temporal evolution of the concentration profiles. This relationship can be observed in Fig. 5a, where the peak concentration decreases as  $\lambda_e$  increases for  $\lambda_e = \{1.40, 1.67, 1.80\}$ . Additionally, lower tortuosity values (i.e.  $\lambda_e = 1.40$ ) result in a shorter time delay of  $\approx 140 \text{ s}$ , while higher tortuosity (i.e.  $\lambda_e = 1.80$ ) leads to a longer time delay of  $\approx 180 \text{ s}$  for the diffusion of molecules through the brain ECS. A similar behaviour can be seen when varying the distance between the point-source MC transmitter and the membrane, i.e., the brain ECS thickness (see Fig. 5b). When transmitting the exosomal tsRNA biomarkers for the smaller brain ECS thickness value (i.e.,  $R_e = 70 \mu\text{m}$ ), we observed the highest peak concentration, with a shorter time delay of  $\approx 125 \text{ s}$ , from the brain ECS thickness chosen values. Conversely, as the transmission distance increased to  $R_e = 80 \mu\text{m}$  and  $R_e = 90 \mu\text{m}$ , we noted a decrease in peak concentration accompanied by a longer time delay  $\approx 145 \text{ s}$  and  $\approx 160 \text{ s}$ , respectively. This trend suggests that longer transmission distances lead to molecular transport delays, resulting in lower peak concentrations. Notably, the peak concentration decrease by a factor of 5, when distances increases from  $R_e = 70 \mu\text{m}$  to  $R_e = 90 \mu\text{m}$ . By comparing Fig. 5a and 5b, we noted that the peak exosomal tsRNA biomarker concentration was higher, and reached quicker, when varying the brain ECS thickness values than modifying this medium tortuosity. This indicates that the brain ECS tortuosity is more detrimental for the exosomal tsRNA biomarker concentration than the medium thickness, becoming the main design factor for transporting molecular signals in the brain ECS.

While crossing the hollow fiber tube's surface to reach the bioengineered sensing cells, the exosomal tsRNA propagation is affected by the membrane's physicochemical factors such as permeability ( $P_m$ ), porosity ( $\phi$ ), and thickness ( $R_m$ ). Here, we vary the values of these parameters and observe their impact on the exosomal tsRNA concentration. First we investigated the impact of permeability ( $P_m$ ), see Fig. 5c, we considered the following values  $P_m = \{0.001, 0.01, 0.1\} \mu\text{m/s}$  in our analysis. We observed that an increase in permeability resulted in increasing the exosomal tsRNA distribution across the membrane, thereby reducing the time it takes to reach the peak concentration ( $\approx 50 \text{ s}$ ), as shown in Fig. 5c. Specifically, the exosomal tsRNA concentration increased by twofold and threefold when increasing the membrane permeability from  $0.001 \mu\text{m/s}$  to  $0.01 \mu\text{m/s}$ , and from  $0.001 \mu\text{m/s}$  to  $0.1 \mu\text{m/s}$ , respectively. Next, we analysed the impact of porosity ( $\phi$ ) on the propagation of exosomal tsRNAs across the membrane. Our analysis considered three porosity values  $\phi = \{0.5, 0.7, 0.9\}$ , as shown in Fig. 5d. We observed that the highest porosity value leads to a rapid increase in exosomal tsRNA concentration, indicating that a larger number of molecules can efficiently pass through the membrane. Conversely, the lowest porosity value requires more time in reaching peak concentration because only a limited number of molecules can pass through the membrane. For the membrane, we found that the peak exosomal tsRNA concentration was increased by factor of approximately 2 and 4 when  $\phi$  increases from 0.5 to 0.7 and from 0.5 to 0.9, respectively. The last physicochemical we analysed for the membrane was its thickness. By observing Fig. 5e, we can see an inverse relationship between the membrane thickness and the exosomal tsRNA peak concentration, and

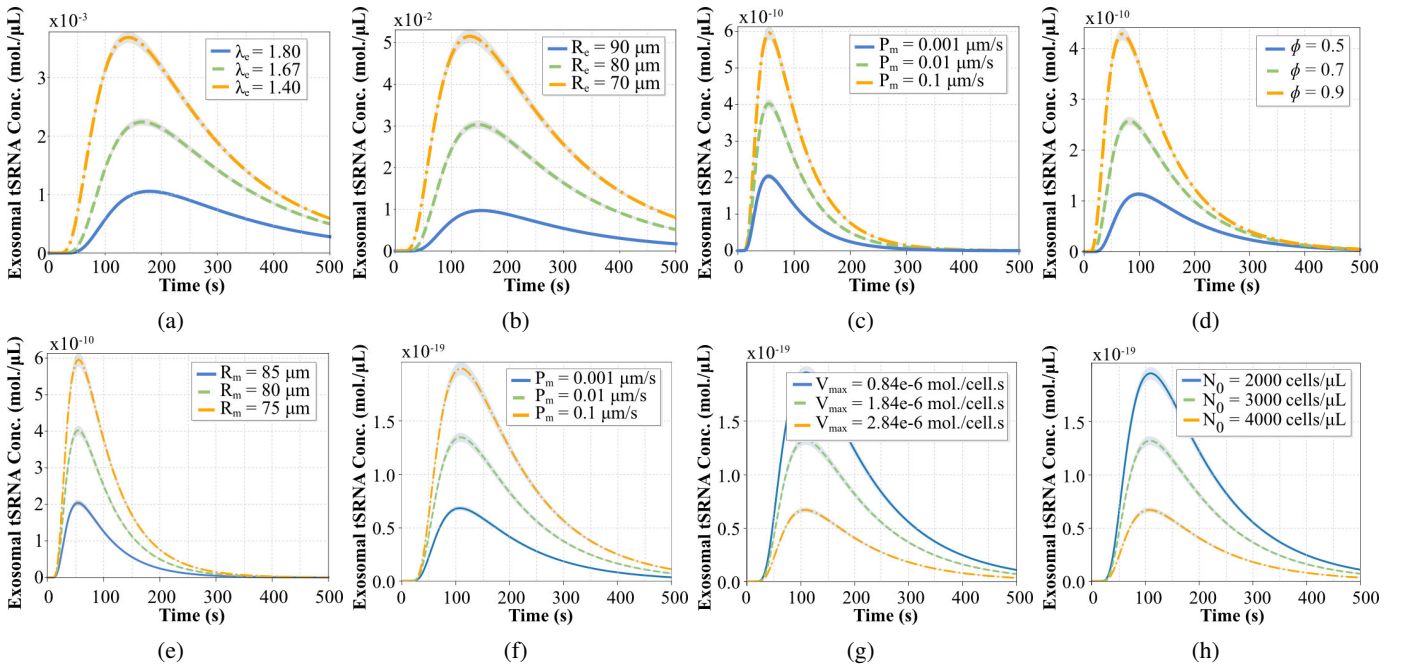


Fig. 5: The impact of physicochemical parameters on exosomal tsRNA concentration profiles. (a) Tortuosity  $\lambda_e$  in the brain ECS. (b) Separation distances  $R_e$  from point-source MC transmitter to the membrane. (c) Membrane permeabilities  $P_m$ . (d) Membrane porosity values  $\phi$ . (e) Membrane wall thickness  $R_m$ . (f) Membrane permeabilities  $P_m$  in the scaffold. (g) Uptake rates  $V_{max}$  in the scaffold. (h) Bioengineered sensing cell densities  $N_0$  in the scaffold. Please note that observations were made at the end of each region (brain ECS, membrane, and scaffold), and each plot shows the mean concentration profile with a 95% confidence interval.

with the time required to reach this maximum value. When the membrane thickness is higher, such as  $R_m = 85 \mu\text{m}$ , the exosomal tsRNA peak concentration decreases, and the time required to reach this peak increases (and the opposite is also true). This observation suggests that a thicker membrane causes more resistance and hinders diffusion, resulting in a gradual accumulation of a small exosomal tsRNA concentration. It is also important to note that a small increase (from  $R_m = 75 \mu\text{m}$  to  $R_m = 85 \mu\text{m}$ ) on the membrane thickness results in a threefold decrease on the exosomal tsRNA peak concentration. From the three physicochemical factors investigated for the membrane, the porosity was the one that showed a greater impact on the exosomal tsRNA concentration. By modifying the porosity we observed a decrease in the overall exosomal tsRNA concentration and an increase in the time required to reach its peak, when compared to the other two physicochemical factors investigated for the membrane. Furthermore, none of the membrane physicochemical factors have a distinct impact on the molecular concentration profiles' peak, but they shorten the time required to reach their maximum exosomal tsRNA concentration values when compared to the brain ECS parameters.

We analysed the impact of different physicochemical properties on the propagation of exosomal tsRNA biomarkers within the scaffold region due to change on the membrane permeability, the maximum uptake rate and the number of bioengineered sensing cells. Fig. 5f illustrates the effect of changing the permeability of the membrane on the received concentration of exosomal tsRNA in the scaffold region. As the membrane permeability ( $P_m$ ) increases, more molecules are able to pass through the membrane and reach the scaffold. Consequently, more molecules reach the bioengineered sensing receiver cells in a shorter period, thereby

reducing the time required to reach their peak concentration (increase by a factor of approximately 2 and 3 when permeability increases from  $0.001 \mu\text{m/s}$  to  $0.01 \mu\text{m/s}$ , and from  $0.001 \mu\text{m/s}$  to  $0.1 \mu\text{m/s}$ , respectively). In this case, while the membrane permeability has a similar effect on the exosomal tsRNA peak concentration when propagating through the membrane, it increases the time required to return to zero when propagating through the scaffold region (i.e., the molecules linger at their destination for a longer period). Next, we analysed the impact of varying uptake rates on the concentration of exosomal tsRNA within the scaffold region. Uptake rate reflects the efficiency of bioengineered sensing receiver cells for absorbing exosomal tsRNA from their surrounding environment. This parameter imposes an interesting trade-off for this system, as a higher maximum uptake rate value means a quicker consumption of the exosomal tsRNA available at the scaffold region, but at the same time it can affect the operation of the bioengineered sensing cells (not all of them would bind enough exosomal tsRNA to activate their functions). Fig. 5g shows an inversely proportional relationship between maximum uptake rate and exosomal tsRNA concentration availability in the region. We obtained a higher exosomal tsRNA peak concentration while assuming a lower maximum uptake rate value (e.g.,  $V_{max} = 0.84e^{-6} \text{ mol./cell.s}$ ), and vice-versa. The final physicochemical factor evaluated for the scaffold region is the bioengineered sensing cells seeding density, which is directly associated with the maximum uptake rate. From Fig. 5h, we observed that for our highest cell density value (i.e.,  $4000 \text{ cells}/\mu\text{L}$ ) we obtained the lowest exosomal tsRNA concentration, indicating a pronounced uptake of biomarkers by the receiver cells. In contrast, for lower bioengineered sensing cell seeding densities, such as  $2000 \text{ cells}/\mu\text{L}$ , resulted in significantly

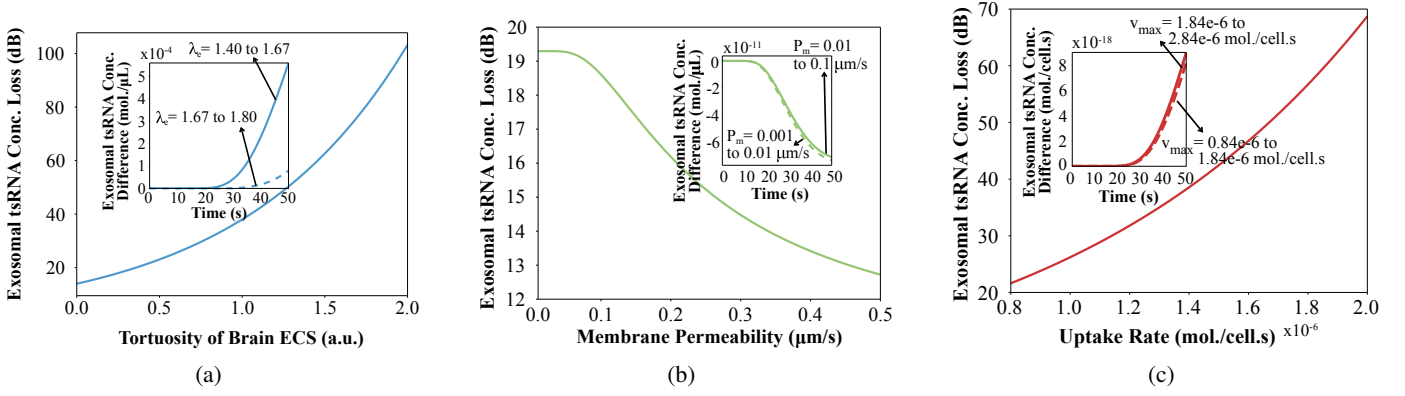


Fig. 6: The exosomal tsRNA concentration loss is assessed for each communication channel in respect to time, tortuosity, membrane permeability and uptake rate. Please note that we plotted the outer graphs using  $t = 50$  s to provide a more accurate representation of the parameter's impact on the exosomal tsRNA concentration loss. (a) Tortuosity  $\lambda_e$  in the brain ECS. (b) Permeability  $P_m$  of the membrane. (c) Uptake rate  $V_{\max}$  in the scaffold region.

higher concentrations. The results obtained for both maximum uptake rate and bioengineered sensing cells seeding density (Fig. 5g and 5h) indicates that a proper control mechanism should be implemented to increase the overall efficiency of this communications system. Furthermore, the difference between the higher and the lower exosomal tsRNA peak concentration is by a factor of three for these two physicochemical factors (considering the values used in our investigation), indicating that they should be defined based on the system requirements to avoid over-consumption of molecular signals.

### B. Channel Propagation Loss Formulation

In our previous analyses we characterised the effects of the physicochemical factors on the temporal dynamics of the exosomal tsRNA concentrations when propagating through the three MC channels investigated in this paper. Due to the observed impact of such factors in the investigated MC system, we utilised (3)-(13) to evaluate the propagation losses in the MC channels. Here we first analysed the individual impact of the physicochemical factors investigated in Section IV-A to formulate mathematical functions that describe the channel propagation loss, and then used these same expressions to observe the combined effect of multiple physicochemical factors on the channel propagation loss.

To obtain the channel propagation losses we extended the methodology applied in Section IV-A to compute the temporal dynamics of the exosomal tsRNA concentration for the main physicochemical factors that affect their diffusion through the MC channel (i.e., tortuosity, membrane permeability and uptake rate), considering a set range of values for these parameters. We calculated the concentration profiles for exosomal tsRNA using the parameter ranges: brain ECS tortuosity ( $\lambda_e = [1.40, 1.67]$  and  $\lambda_e = [1.67, 1.80]$ ), membrane permeability ( $P_m = [0.001, 0.01] \mu\text{m/s}$  and  $P_m = [0.01, 0.1] \mu\text{m/s}$ ), and uptake rate ( $V_{\max} = [0.84, 1.84]e^{-6} \text{ mol./cell}\cdot\text{s}$  and  $V_{\max} = [1.84, 2.84]e^{-6} \text{ mol./cell}\cdot\text{s}$ ). Then we took the differences between the exosomal tsRNA concentrations obtained using the maximum and minimum values for each parameter range. In this context, 'maximum' refers to the concentration profile derived from the highest value within each parameter's range, while 'minimum' refers to the profile calculated using the lowest

value. For the brain ECS, the tortuosity has the most impact on the exosomal tsRNA concentration, which will reduce the rate of molecular movement within this MC channel and lead to loss of the diffused biomarkers. When computing the temporal dynamics for two ranges of values for this physicochemical factor ( $\lambda_e = [1.40, 1.67]$  and  $\lambda_e = [1.67, 1.80]$ ), we observed that the exosomal tsRNA concentration difference follows an exponential growth (see inner plot of Fig. 6a). Therefore, we obtained the tortuosity-induced loss ( $PL_e$ ) based on [44–46] as follows,

$$PL_e(\text{dB}) = L_e \cdot 10 \log_{10}(R_e), \quad (14)$$

where,  $L_e = e^{\lambda_e}$  is the tortuosity-induced loss factor. Using (14), we calculated the exosomal tsRNA concentration loss which is depicted in Fig. 6a. From these result, we observed that at the lower tortuosity value, the ( $PL_e$ ) model showed minimal concentration loss. However, at higher tortuosity values, there was a substantial increase in concentration loss—approximately 10 times greater than that observed at lower tortuosity level. This suggests that beyond a certain point, the structural complexity of the ECS significantly hinders the movement of molecules. These findings indicates that tortuosity is an important parameter for ensuring the efficient propagation of molecules within a brain ECS. Therefore, it is important to consider and control tortuosity to optimize the transport of biomarkers within communication channel.

During propagation along the membrane, the exosomal tsRNA can be lost due to several physicochemical factors, including the membrane's thickness, porosity, permeability, tortuosity and diffusion coefficient. Based on the results from Section IV-A and following a similar methodology applied to compute  $PL_m$ , we considered two ranges of values for the membrane permeability ( $P_m = [0.001, 0.01] \mu\text{m/s}$  and  $P_m = [0.01, 0.1] \mu\text{m/s}$ ) and observe that the exosomal tsRNA concentration difference can be represented by a sigmoid function (see inner plot of Fig. 6b). Moreover, due to the number of physicochemical factors affecting the diffusion of the exosomal tsRNA molecules, we formulated the propagation loss for this MC channel as the measure of the collective impact of these parameters on the exosomal tsRNAs' propagation as [44–46],

$$PL_m(\text{dB}) = L_m \cdot 10 \cdot \log_{10}(R_m), \quad (15)$$

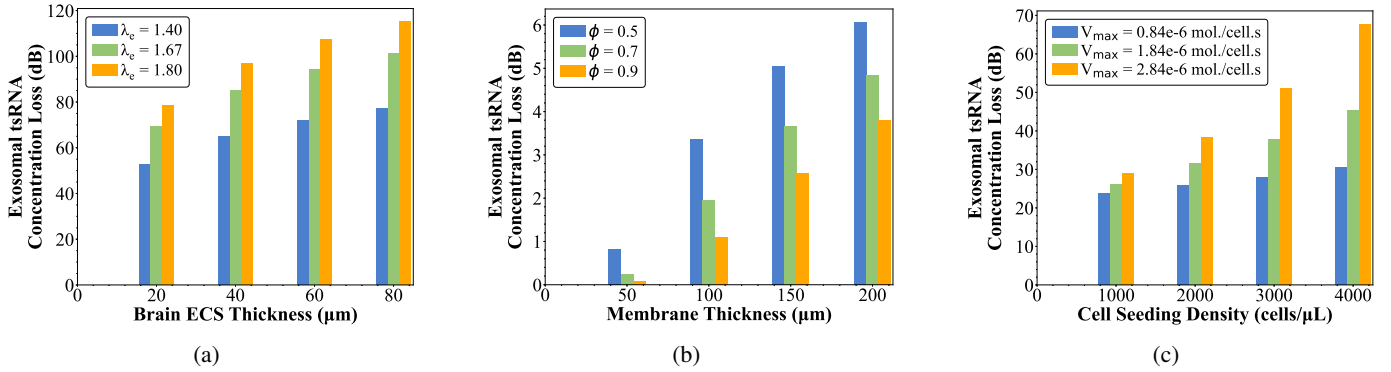


Fig. 7: Exosomal tsRNA concentration loss for different physicochemical parameter values. (a) Tortuosity  $\lambda_e$  and brain ECS thickness. (b) Porosity  $\phi$  and membrane thickness. (c) Uptake rate  $V_{\text{max}}$  and cell seeding density.

where  $L_m = \frac{1}{1+e^{-\lambda_m \cdot R_m}}$  is the membrane loss factor,  $\lambda_m = (D_s \phi) / (P_m \cdot R_m)$  is the tortuosity factor for this MC channel. It is obtained by combining the membrane's permeability and diffusion coefficient equations, see Section III-B. By evaluating (15), we observed that the exosomal tsRNA concentration loss decreased sigmoidally when the permeability ( $P_m$ ) increased from  $0.01 \mu\text{m/s}$  to  $0.5 \mu\text{m/s}$ . Specifically, a significant decrease in concentration loss was observed at the permeability  $0.5 \mu\text{m/s}$ , where the concentration loss decreased by approximately 32%. These findings contributed to our understanding of how the permeability parameter impacted molecular diffusion, offering valuable implications for the hollow fiber tube's membrane design (e.g., choice of the biomaterial and techniques to prepare membranes with the permeability required for the desired MC system).

The propagation of exosomal tsRNA in the scaffold region is affected by the presence of bioengineered sensing cells, as shown in Fig. 5g and 5h. The consumption of exosomal tsRNA by these cells within the scaffold contributes significantly to the overall loss of molecules during propagation along the channel. Applying a similar approach used to formulate the channel propagation loss on the other MC channels, we selected two ranges of values for the maximum uptake rate  $V_{\text{max}} = [0.84, 1.84]e^{-6}$  mol./cell.s and  $V_{\text{max}} = [1.84, 2.84]e^{-6}$  mol./cell.s and observed the temporal dynamics of the exosomal tsRNA concentration difference, which can be represented as an exponential growth, see inner plot of Fig. 6c. Therefore, we defined a loss factor that considers the impact of bioengineered sensing cells on molecule uptake to express the channel propagation loss for the scaffold region as [44–46],

$$PL_s(\text{dB}) = L_s \cdot 10 \cdot \log_{10}(R_s), \quad (16)$$

where  $L_s = e^v$  is the scaffold loss factor. The consumption coefficient, represented as  $v = (N_0 \cdot V_{\text{max}}) / k_H$ , remains constant and is determined by the properties of the MC channel components, see Section III-C. Using (16), we calculated the exosomal tsRNA concentration loss, which is depicted in Fig. 6c. From these result, we observed that at the uptake rate of  $0.8e^{-6}$  mol./cell.s, the  $PL_s$  model showed minimal concentration loss. However, at  $2.0e^{-6}$  mol./cell.s uptake rate value, there was a significant increase in concentration loss—approximately 3 times higher than that observed at lower uptake rate. This indicates that higher uptake rates substantially reduce the availability of exosomal tsRNA in the scaffold region, due to quicker absorption

by bioengineered sensing cells. Therefore, a careful balance is necessary to achieve optimal uptake by bioengineered sensing cells while maintaining sufficient levels of exosomal tsRNA in the scaffold region for effective cell function.

### C. Channel Propagation Loss Analysis

Using (14)-(16) we analysed the performance for the exosomal tsRNA diffusion in all three MC channels. For the brain ECS, we investigated the impact of both tortuosity ( $\lambda_e$ ) and thickness ( $R_e$ ) on the propagation of exosomal tsRNA molecules traveling through the brain ECS region, as shown in Fig. 7a. Specifically, we considered four different brain ECS thickness values as  $[20, 40, 60, 80] \mu\text{m}$  and tortuosity values of  $[1.40, 1.67, 1.80]$ . From Fig. 7a, we observed that, as the ECS thickness increases, there is a corresponding rise in concentration loss. For instance, when comparing an ECS thickness of  $20 \mu\text{m}$  with  $80 \mu\text{m}$ , the later showed a significantly higher loss, likely due to the increased resistance and hindered diffusion through thicker ECS region. Similarly, when analysing the tortuosity values, a higher value of  $\lambda_e = 1.80$  resulted in increased loss compared to  $\lambda_e = 1.40$ . This suggests that more convoluted pathways within the ECS hinders the propagation of tsRNA molecules, contributing to higher loss, consistent with the results shown in Fig. 6a. These findings provide insights into the factors influencing molecular transport in the brain and can help in optimizing the performance of devices implanted in the brain by balancing the thickness and tortuosity of the brain ECS.

Next, we investigated the impact of both porosity ( $\phi$ ) and thickness ( $R_m$ ) on the propagation of exosomal tsRNA molecules traveling through the membrane region, as shown in Fig. 7b. We considered four different membrane thickness values as  $[50, 100, 150, 200] \mu\text{m}$  and porosity values of  $[0.5, 0.7, 0.9]$ . From Fig. 7b, it is observed that as thickness increases, there is rise in concentration loss due to the hindered diffusion of molecules through thicker membranes. However, a higher porosity value (e.g.,  $\phi = 0.9$ ) counteracts this trend and reduces loss by approximately 33%, resulting in an increase in the number of molecules passing through the membrane. This result can provide insights on the factors influencing molecular transport through a device implanted in the brain. Furthermore, this indicates that the membrane porosity and membrane thickness becoming the main design parameters for transporting molecular signals to the bioengineered sensing cells and have major impact on overall performance of the system. It is also important to

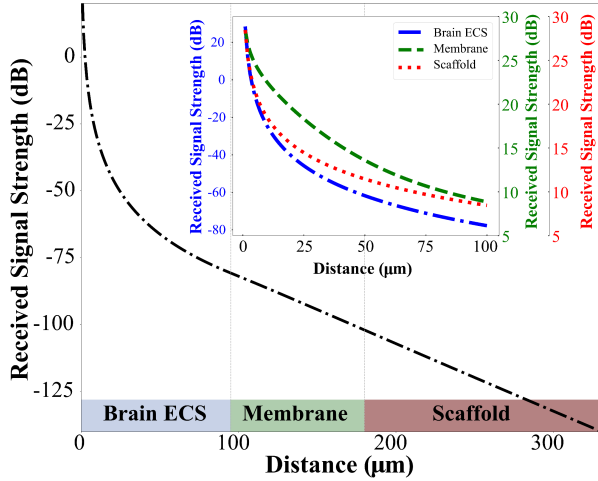


Fig. 8: Link budget analysis in terms of received signal strength for each region (observed using  $t = 50$  s). Please note that we plotted the inner graph to show the received signal strength for the same distance across each communication channel, highlighting the distinct effects on the link budget.

find a good balance between the thickness of the membrane and its porosity to optimize the performance of this molecular transport.

In Fig. 7c, we analyse the impact of both the bioengineered sensing cells seeding density ( $N_0$ ) and uptake rate ( $V_{\max}$ ) of bioengineered sensing cells on the propagation of exosomal tsRNA biomarkers traveling through the scaffold region. For this analysis, we considered four cell seeding density values  $[1000, 2000, 3000, 4000]$  cells/ $\mu\text{L}$  and uptake rates of  $[0.84, 1.84, 2.84]e^{-6}$  mol./cell·s. It is observed that as the cell seeding density value increases from  $N_0 = 1000$  cells/ $\mu\text{L}$  to  $N_0 = 4000$  cells/ $\mu\text{L}$ , there is rise in concentration loss due to the greater uptake of tsRNA molecules by the increased number of cells in the scaffold, resulting in a reduction in overall molecule concentration. At the highest uptake rate (i.e.,  $V_{\max} = 2.84e^{-6}$  mol./cell·s), a higher concentration loss is observed, indicating that a higher uptake rate leads to a more rapid removal of tsRNA molecules from the scaffold, further contributing to the reduction in molecular concentration. These findings emphasize the impact of bioengineered sensing cell density and uptake rate on exosomal tsRNA biomarker propagation loss. By optimizing these parameters, we can enhance the efficiency and accuracy of biomarker detection, which in turn could improve diagnostic and therapeutic applications.

#### D. Molecular Link Budget Formulation and Analysis

Inspired by typical communications systems, which have their link budget formulated based on the combined effect of the signal power from transmitter, receiver, gains and losses, we defined the link budget for our investigated MC system as [47],

$$S_{R_x}(\text{dB}) = S_{T_x}(\text{dB}) + G_{T_x}(\text{dB}) - PL_T(\text{dB}) + G_{R_x}(\text{dB}), \quad (17)$$

where  $S_{R_x}$  is the received molecular signal strength;  $G_{T_x}$  and  $G_{R_x}$  are the gains of the transmitting and receiving cells, respectively; and  $PL_T(\text{dB})$  is the total loss for the proposed heterogeneous MC channel as described in [47], and is given

by the combined propagation losses formulated in Section IV-B. Therefore,

$$PL_T(\text{dB}) = PL_e(\text{dB}) + PL_m(\text{dB}) + PL_s(\text{dB}). \quad (18)$$

We used (18) to observe how these heterogeneous MC channels affect the molecular transport of exosomal tsRNA molecules. In this link budget analysis, we considered the initial transmission of  $Q = 700$  molecules from neuronal cells ( $T_x$ ) in the brain ECS at  $R_e = 0 \mu\text{m}$  and  $t = 0$  s to the bioengineered sensing cells ( $R_x$ ) located at the distance of  $180 \mu\text{m}$  in the scaffold region, through device membrane wall. Fig. 8 illustrates that as these molecules traverse from brain ECS towards the bioengineered sensing cells, a notable decrease in received signal strength (i.e. exosomal tsRNA concentration) is observed, indicating an approximate 8-fold loss in the MC link. This reduction in signal strength is due to the physicochemical factors investigated in the previous sections. We believe that by addressing these channel propagation losses and refining design parameters based on our findings, bioengineers could improve the accuracy and reliability of implantable biosensors for the prediction of epileptic seizures.

## V. CONCLUSION

In this paper, we designed a MC model based on wet-lab experimental data to characterize the propagation of epileptic biomarkers (i.e. exosomal tsRNAs) within the heterogeneous fluidic environment. Our model aims to facilitate the design of biosensing devices for the prediction of epileptic seizures by characterizing the propagation of these biomarkers from neuronal cells in the brain ECS to a bioengineered implant. In this work, we investigated the influence of various physicochemical characteristics, including tortuosity, membrane thickness, permeability, porosity, bioengineered cell seeding density, and uptake rate within each channel, on the propagation of molecules. In our study, we used two performance metrics for evaluation of the communication system: propagation loss and molecular communication (MC) link budget. These metrics are used to explore the impact of different properties of heterogeneous channels (i.e., brain ECS, membrane, and hydrogel) on both the propagation of molecules and the received molecular signals by bioengineered sensing cells in the context of prediction of epileptic seizures. Our findings indicate that concentration loss increases with increased tortuosity of the brain ECS and membrane thickness. However, higher membrane permeability and porosity improve molecular propagation, thus reducing loss. Furthermore, higher cell seeding density and uptake rates result in greater concentration loss, because the increased density and uptake rate lead to a more rapid removal of tsRNA molecules from the scaffold, further contributing to the reduction in molecular concentration. In addition, the strength of the received signal demonstrates a decrease as these molecules traverse the brain ECS toward bioengineered sensing cells, indicating an approximate 8-fold loss in the molecular communication (MC) link. The obtained results lay the foundation for key design parameters that are needed in designing and optimizing bioengineered devices for prediction of epileptic seizures and for other neurological diseases.

In future work, we plan to extend this research to observe other molecular diffusion scenarios by allowing molecules to enter from various locations within the cylinder, particularly near the ends of the tube (i.e., device). For this, we will incorporate both

radial and axial molecular flow to capture the spatial complexity of molecular propagation and its influence on the diffusion dynamics and detection capabilities of bioengineered sensing cells. Additionally, we aim to find optimal parameters that can improve the detection capability of bioengineered sensing cells and their response sensitivity. This can result in the development of more efficient biosensing systems capable of detecting and predicting neurological disorders with higher accuracy and faster response times.

#### REFERENCES

- [1] Kirsten M Fiest, Khara M Sauro, Samuel Wiebe, Scott B Patten, Churl-Su Kwon, Jonathan Dykeman, Tamara Pringsheim, Diane L Lorenzetti, and Nathalie Jetté. Prevalence and incidence of epilepsy: a systematic review and meta-analysis of international studies. *Neurology*, 88(3):296–303, 2017.
- [2] Anssi Pelkonen, Ropafadzo Mzezewa, Lassi Sukki, Tomi Ryyänen, Joose Kreutzer, Tanja Hyvärinen, Andrey Vinogradov, Laura Aarnos, Jukka Leikkala, Pasi Kallio, et al. A modular brain-on-a-chip for modelling epileptic seizures with functionally connected human neuronal networks. *Biosensors and Bioelectronics*, 168:112553, 2020.
- [3] Carl E Stafstrom and Lionel Carmant. Seizures and epilepsy: an overview for neuroscientists. *Cold Spring Harbor perspectives in medicine*, 5(6), 2015.
- [4] Michele Simonato, Denes V Agoston, Amy Brooks-Kayal, Chris Dulla, Brandy Fureman, David C Henshall, Asla Pitkänen, William H Theodore, Roy E Twyman, Firas H Kobeissy, et al. Identification of clinically relevant biomarkers of epileptogenesis—a strategic roadmap. *Nature Reviews Neurology*, 17(4):231–242, 2021.
- [5] Marion C Hogg, Rana Raoof, Hany El Nagggar, Naser Monsefi, Norman Delanty, Donncha F O’Brien, Sebastian Bauer, Felix Rosenow, David C Henshall, Jochen HM Prehn, et al. Elevation of plasma trna fragments precedes seizures in human epilepsy. *The Journal of clinical investigation*, 129(7):2946–2951, 2019.
- [6] Steven G Fagan, Mark Helm, and Jochen HM Prehn. trna-derived fragments: A new class of non-coding rna with key roles in nervous system function and dysfunction. *Progress in Neurobiology*, 205:102118, 2021.
- [7] Huinan Li, Cheng Wu, Rodolfo Aramayo, Matthew S Sachs, and Mark L Harlow. Synaptic vesicles contain small ribonucleic acids (srnas) including transfer rna fragments (trfrna) and micrnas (mirna). *Scientific reports*, 5(1):14918, 2015.
- [8] Zhiyun Wei, Arsen O Batagov, Sergio Schinelli, Jintu Wang, Yang Wang, Rachid El Fatimy, Rosalia Rabinovsky, Leonora Balaj, Clark C Chen, Fred Hochberg, et al. Coding and noncoding landscape of extracellular rna released by human glioma stem cells. *Nature communications*, 8(1):1145, 2017.
- [9] Xinxin Lv, Ruorui Zhang, Shanshan Li, and Xin Jin. trna modifications and dysregulation: Implications for brain diseases. *Brain Sciences*, 14(7):633, 2024.
- [10] Shivani Tiwari, Varsha Sharma, Mubarak Mujawar, Yogendra Kumar Mishra, Ajeet Kaushik, and Anujit Ghosal. Biosensors for epilepsy management: state-of-art and future aspects. *Sensors*, 19(7):1525, 2019.
- [11] Min Wei, Peihua Lin, Ying Chen, Ji Young Lee, Lingxiao Zhang, Fangyuan Li, and Daishun Ling. Applications of ion level nanosensors for neuroscience research. *Nanomedicine*, 15(29):2871–2881, 2020.
- [12] Muneer M Al-Zubi, Ananda S Mohan, Peter Plapper, and Sai Ho Ling. Intrabody molecular communication via blood-tissue barrier for internet of bio-nano things. *IEEE Internet of Things Journal*, 9(21):21802–21810, 2022.
- [13] Qing Zheng, Hao Wu, Nan Wang, Rui Yan, Yuehui Ma, Weijun Guang, Junzhong Wang, and Kejian Ding. Graphene-based biosensors for biomolecules detection. *Current Nanoscience*, 10(5):627–637, 2014.
- [14] Hamidreza Arjmandi, Mohamad Zoofaghari, Mitra Rezaei, Kajsa Kanebratt, Liisa Vilen, David Janzen, Peter Genemark, and Adam Noel. Diffusive molecular communication with a spheroidal receiver for organ-on-chip systems. *arXiv preprint arXiv:2302.09265*, 2023.
- [15] Na-Rae Kim, Andrew W Eckford, and Chan-Byoung Chae. Symbol interval optimization for molecular communication with drift. *IEEE transactions on nanobioscience*, 13(3):223–229, 2014.
- [16] Deniz Kilinc and Ozgur B Akan. Receiver design for molecular communication. *IEEE Journal on Selected Areas in Communications*, 31(12):705–714, 2013.
- [17] Massimiliano Pierobon and Ian F Akyildiz. A statistical-physical model of interference in diffusion-based molecular nanonetworks. *IEEE Transactions on communications*, 62(6):2085–2095, 2014.
- [18] Saizalmursidi Md Mustam, Sharifah Kamilah Syed Yusof, and Samad Nejatian. Multilayer diffusion-based molecular communication. *Transactions on Emerging Telecommunications Technologies*, 28(1):e2935, 2017.
- [19] Saizalmursidi Md Mustam, Sharifah K Syed-Yusof, and Suleiman Zubair. Capacity and delay spread in multilayer diffusion-based molecular communication (dbmc) channel. *IEEE transactions on nanobioscience*, 15(7):599–612, 2016.
- [20] Muneer M Al-Zu’bi and Ananda Mohan Sanagavarapu. Modeling a composite molecular communication channel. *IEEE Transactions on Communications*, 66(8):3420–3433, 2018.
- [21] NS Abdullah and DB Das. Modelling nutrient transport in hollow fibre membrane bioreactor for growing bone tissue with consideration of multi-component interactions. *Chemical Engineering Science*, 62(21):5821–5839, 2007.
- [22] Eva Syková and Charles Nicholson. Diffusion in brain extracellular space. *Physiological reviews*, 88(4):1277–1340, 2008.
- [23] Mladen Veletić, Michael Taynnan Barros, Ilango Balasingham, and Sasitharan Balasubramaniam. A molecular communication model of exosome-mediated brain drug delivery. In *Proceedings of the Sixth Annual ACM International Conference on Nanoscale Computing and Communication*, pages 1–7, 2019.
- [24] Shuai Wang, Hazwani Suhaimi, Mostafa Mabrouk, Stella Georgiadou, John P Ward, and Diganta B Das. Effects of scaffold pore morphologies on glucose transport limitations in hollow fibre membrane bioreactor for bone tissue engineering: experiments and numerical modelling. *Membranes*, 11(4):257, 2021.
- [25] Efreem Curcio, L De Bartolo, G Barbieri, M Rende, L Giorno, S Morelli, and E Drioli. Diffusive and convective

- transport through hollow fiber membranes for liver cell culture. *Journal of biotechnology*, 117(3):309–321, 2005.
- [26] Jeffrey Capadona, George Hoeflerlin, Sarah Grabinski, Lindsey Druschel, Jonathan Duncan, Grace Burkhart, Gwendolyn Weagraff, Alice Lee, Christopher Hong, Meera Bambrro, et al. Bacteria invade the brain following sterile intracortical microelectrode implantation. *Research Square*, 2024.
- [27] Chuying Ma, Ethan Gerhard, Qiaoling Lin, Silun Xia, April Dawn Armstrong, and Jian Yang. In vitro cyto-compatibility evaluation of poly (octamethylene citrate) monomers toward their use in orthopedic regenerative engineering. *Bioactive materials*, 3(1):19–27, 2018.
- [28] Haluk Beyenal and Abdurrahman Tanyolaç. A mathematical model for hollow fiber biofilm reactors. *The Chemical Engineering Journal and the Biochemical Engineering Journal*, 56(1):B53–B59, 1994.
- [29] John P Tharakan and Pao C Chau. A radial flow hollow fiber bioreactor for the large-scale culture of mammalian cells. *Biotechnology and Bioengineering*, 28(3):329–342, 1986.
- [30] Mohamed Hayek. An exact solution for a nonlinear diffusion equation in a radially symmetric inhomogeneous medium. *Computers & Mathematics with Applications*, 68(12):1751–1757, 2014.
- [31] Maciej Matyka, Arzhang Khalili, and Zbigniew Koza. Tortuosity-porosity relation in porous media flow. *Physical Review E*, 78(2):026306, 2008.
- [32] Hazwani Suhaimi, Shuai Wang, Tom Thornton, and Diganta Bhusan Das. On glucose diffusivity of tissue engineering membranes and scaffolds. *Chemical Engineering Science*, 126:244–256, 2015.
- [33] Surendra Singh Rathore, Balkrishna Mehta, Pradeep Kumar, and Mohammad Asfer. Flow characterization in triply periodic minimal surface (tpms)-based porous geometries: Part 1—hydrodynamics. *Transport in Porous Media*, 146(3):669–701, 2023.
- [34] C de Santiago and M Raya. Study of the porosity features of lightweight expanded clay aggregates by means of helium pycnometry and mercury porosimetry. In *Cities and their underground environment. Proc. of II European Conference of the International Association for Engineering Geology. EUROENGE*, 2008.
- [35] Helene Roberge, Philippe Moreau, Estelle Couallier, and Patricia Abellan. Determination of the key structural factors affecting permeability and selectivity of pan and pes polymeric filtration membranes using 3d fib/sem. *Journal of Membrane Science*, 653:120530, 2022.
- [36] Zulfida Mohamad Hafis Mohd Shafie, Abdul Latif Ahmad, Siew Chun Low, Sabine Rode, and Bouchra Bellaissaoui. Lithium chloride (licl)-modified polyethersulfone (pes) substrate surface pore architectures on thin poly (dimethyl-siloxane)(pdms) dense layer formation and the composite membrane's performance in gas separation. *RSC advances*, 10(16):9500–9511, 2020.
- [37] Amir Muhammad, Mohammad Younas, and Mashallah Rezakazemi. Quasi-dynamic modeling of dispersion-free extraction of aroma compounds using hollow fiber membrane contactor. *Chemical Engineering Research and Design*, 127:52–61, 2017.
- [38] Davod Mohebbi-Kalhari, Amin Behzadmehr, Charles J Doillon, and Afra Hadjizadeh. Computational modeling of adherent cell growth in a hollow-fiber membrane bioreactor for large-scale 3-d bone tissue engineering. *Journal of Artificial Organs*, 15:250–265, 2012.
- [39] Shunji Yunoki, Yoshimi Ohyabu, and Hirotsuke Hatayama. Temperature-responsive gelation of type i collagen solutions involving fibril formation and genipin crosslinking as a potential injectable hydrogel. *International journal of biomaterials*, 2013(1):620765, 2013.
- [40] Marjan Shayegan and Nancy R Forde. Microrheological characterization of collagen systems: from molecular solutions to fibrillar gels. *PloS one*, 8(8):e70590, 2013.
- [41] Elisabeth D Chang, Christer Hogstrand, Thomas H Miller, Stewart F Owen, and Nic R Bury. The use of molecular descriptors to model pharmaceutical uptake by a fish primary gill cell culture epithelium. *Environmental science & technology*, 53(3):1576–1584, 2018.
- [42] Fang Zhou, Pearl Ebea, Ezra Mutai, Haichuan Wang, Sonal Sukreet, Shya Navazesh, Haluk Dogan, Wenhao Li, Juan Cui, Peng Ji, et al. Small extracellular vesicles in milk cross the blood-brain barrier in murine cerebral cortex endothelial cells and promote dendritic complexity in the hippocampus and brain function in c57bl/6j mice. *Frontiers in nutrition*, 9:838543, 2022.
- [43] PPBM Diana Mindrila, Phoebe Balentyne, and How Confidence Intervals Behave. Confidence intervals. in *The Basic Practice of Statistics*, 2013.
- [44] Xavier Timoneda, Albert Cabellos-Aparicio, Dionysios Manassis, Eduard Alarcón, and Sergi Abadal. Channel characterization for chip-scale wireless communications within computing packages. In *2018 Twelfth IEEE/ACM International Symposium on Networks-on-Chip (NOCS)*, pages 1–8. IEEE, 2018.
- [45] Virginia Chika Ebhota, Joseph Isabona, and Viranjay M Srivastava. Base line knowledge on propagation modelling and prediction techniques in wireless communication networks. *Journal of Engineering and Applied Sciences*, 13(7):1919–1934, 2018.
- [46] Kamran Sayrafian-Pour, Wen-Bin Yang, John Hagedorn, Judith Terrill, Kamyra Yekeh Yazdandoost, and Kiyoshi Hamaguchi. Channel models for medical implant communication. *International Journal of Wireless Information Networks*, 17:105–112, 2010.
- [47] Pedram Johari, Honey Pandey, and Josep M Jornet. Interconnecting wearable devices with nano-biosensing implants through optical wireless communications. In *Optical Diagnostics and Sensing XVIII: Toward Point-of-Care Diagnostics*, volume 10501, pages 281–292. SPIE, 2018.



**Aiman Khalil** received her B.E degree in Computer Systems from Mehran University of Engineering and Technology, Pakistan, in 2018. She is currently pursuing a PhD degree with the Department of Computing and Mathematics at South East Technological University, Ireland. Her current research interests include molecular communications, artificial intelligence and biosensing.



**Kurt Pumares** received the BSc degree in Mathematics at University of the Philippines Cebu, Cebu City, Philippines in 2015 and the MSc degree in Applied Mathematics at University of the Philippines Diliman, Quezon City, Philippines in 2018. He is currently a PhD student at Walton Institute, South East Technological University, Waterford City, Ireland. His research interests include computational synthetic biology, molecular communications, and molecular machine learning.



**Anne Skogberg** received her master's degree in cell and tissue engineering from the University of Tampere, Finland, in 2010, and her D.Sc. degree from the Faculty of Medicine and Health Technology at Tampere University in 2023. During her academic career, her research focused on nanocellulose and its applications in biomedical fields. She is currently working in the industry.



**Pasi Kallio** received an M.Sc. degree in electrical engineering and a D.Tech. degree in automation engineering from Tampere University of Technology (TUT), Finland, in 1994 and 2002, respectively. From 2008 to 2018, he served a Professor of Automation Engineering in the Faculty of Biomedical Sciences and Engineering at TUT. Since 2019, he has been a Professor of Biomedical Micro and Nanodevices in the Faculty of Medicine and Health Technology at Tampere University, where he also served as Vice Dean for Research from 2019 to 2023. He has authored

more than 190 articles and holds 16 patent applications. His current research interests include microfluidics, microsensors, microrobotics, and their automation in microphysiological systems, olfactory displays and fibrous material testing applications. Professor Kallio was the Chair of the IEEE Finland Section from 2012 to 2013. He was a recipient of the Finnish Automation Society Award in 2009 and has co-founded three start-up companies.



**Deirdre Kilbane** received her Bachelors of Science (Experimental Physics) and Ph.D. (Mathematical Physics) degrees from University College Dublin, Ireland, and National University of Ireland Maynooth, respectively. She is currently Director of Research at Walton Institute for Information and Communication Systems Science, South East Technological University, Ireland. She was previously a Marie Curie Fellow in the University of Kaiserslautern, Germany, and a recipient of two Science Foundation Ireland Industry Fellowships. Deirdre has authored and co-authored

over 50 journal and conference papers and is a reviewer for many journals. Her current research interests include artificial intelligence, nano-optics, biosensing, and quantum communication.



**Daniel P. Martins** (Member, IEEE) is currently an Assistant Professor and Curriculum Development Director with the School of Computer Science and Electronic Engineering, University of Essex, UK. Daniel received his PhD from Waterford Institute of Technology, and his research interests include cellular signal processing, biosensing, molecular/nano communications and agent-based simulations of biological systems.